

Deep Bayesian Uncertainty Estimation for Adaptation and Self-Annotation of Food Packaging Images

Fabio De Sousa Ribeiro · Francesco Calivá · Mark Swainson ·
Kjartan Gudmundsson · Georgios Leontidis · Stefanos Kollias

Received: date / Accepted: date

Abstract Food packaging labels provide important information for public health, such as allergens and *use-by* dates. Off-the-shelf Optical Character Verification (OCV) systems are good solutions for automating food label quality assessments, but are known to underperform on complex data. This paper proposes a Deep Learning based system that can identify inadequate images for OCV, due to their poor label quality, by employing state-of-the-art Convolutional Neural Network (CNN) architectures, and practical Bayesian inference techniques for automatic self-annotation. We propose a practical domain adaptation procedure based on k -means clustering of CNN latent variables, followed by a k -Nearest Neighbour classification for handling high label variability between different dataset distributions. Moreover, Supervised Learning has proven useful in such systems but manual annotation of large amounts of data is usually required. This is practically intractable in most real world problems due to time/labour constraints. In an attempt to address this issue, we introduce a self-annotating prediction model based on Self-Training of a Bayesian CNN, that leverages modern variational inference methods of deep models. In this context, we propose a new *inverse uncertainty weighting* technique that encourages the Self-

Training model to learn from more informative data over time, potentially preventing it from becoming *lazy* by only selecting easy examples to learn from. An experimental study is presented illustrating the superior performance of the proposed approach over standard Self-Training, and highlighting the importance of predictive uncertainty estimates in safety-critical domains.

Keywords Bayesian convolutional neural network · variational inference · self-training · uncertainty weighting · deep learning · clustering · representation learning · adaptation · optical character verification

1 Introduction

Systems of national and global food supply are often complex and multifaceted, characterised by multiple stages of processing and distribution. In the European Union, food production is the largest manufacturing sector accounting for 13.3% of the total EU-28 manufacturing sector with a reported turnover of 945 billion. Whilst food availability is a primary concern in developing nations and food quality/value a focal point in more affluent societies, food safety is a requirement that is common across all food supply chains. Food safety in the sector is typically underpinned by food science and technology and assured by a combination of operational control systems and procedures including Good Manufacturing Practice and Hazard Analysis & Critical Control Point. Pre-packaged food products, which are incorrectly labelled (e.g. bearing an incorrect or illegible *use-by* date), result in product recalls, as the fault/issue could cause a food safety incident, such as food poisoning due to the consumption of the product which is past its safe *use-by* date for consumption. These recalls

Fabio De Sousa Ribeiro, Francesco Calivá,
Georgios Leontidis, and Stefanos Kollias
MLearn Group
School of Computer Science
University of Lincoln
E-mail: {fdesousaribeiro, fcaliva,
gleontidis, skollias}@lincoln.ac.uk

Mark Swainson, Kjartan Gudmundsson
National Centre for Food Manufacturing
Holbeach Technology Park
E-mail: {mswainson, kgudmundsson}@lincoln.ac.uk

are usually at very high financial cost to food manufacturers, often compromising their reputation. Recurring root causes for mistakes resulting in label faults on food packaging are many and varied, but are primarily attributed to human error and equipment faults. In most cases, a human operator performs a check, by either manually picking a pack from the line for inspection, or verifying it through an image captured of the pack. However, these methods create mundane and repetitive tasks, placing the operator in an error-prone working environment. Moreover, these methods do not offer any statistically significant data for analysis by suppliers. For example, checking the correctness of a pack once every 5 minutes (when the line is running at 100 packs per minute) enhances the risk of missing a fault across the other 499 packs processed during the check interval. Another approach to control date codes is to use Optical Character Verification (OCV). This involves a supervisory system holding the correct date code string and transferring it to both the printer and the vision system. The latter will then verify its read, and depending on the result, appropriate actions are taken. However, OCV systems rely on consistency in date code format, packaging and camera view angle. This consistency tends to be hard to achieve in the food & drink manufacturing environment, and therefore there is a great need for a more robust solution. OCV systems generally rely on the availability of accurately labelled data to be utilised for training. However, the labelling process is time consuming, expensive and requires expertise.

The ability to label data sets with limited supervision proves ideal, as this can reduce the volume of data to manually annotate. The latter is reflected in reduced costs and product production time. On this regard, deep learning based architectures can be capable of generalising their knowledge obtained from smaller data sets to larger ones. Nevertheless, training traditional deep architectures, suffers from the need of availability of large amounts of labelled data. Such limitations can be reduced by adopting recent Bayesian approaches to Convolutional Neural Networks (BCNNs), which provide new opportunities to produce self-annotating systems. To address these issues, we expand on earlier work in OCV systems [1], and relieve the time-consuming task of manual annotation. We propose an approach orthogonal to [2], in which we employ recent approximate variational inference techniques for deep models to estimate uncertainty in supervised Self-Training. As explained in greater detail in the following sections, we utilise estimated aleatoric and epistemic uncertainties to predict pseudo labels for our data, and select points of higher confidence in an automated manner. We also

offer ways to mitigate propagating errors by including a confidence penalty in the log likelihood loss, and introduce an adaptive sample-wise weighting scheme that controls the influence of predicted pseudo labels over gradient updates based on uncertainty estimates. It is important to note that our approach was developed to perform well on our particular application domain, but nonetheless it could easily be extended to generalise to other types of problems.

2 Related Work

Deep Learning (DL) model’s ability to learn complex abstract representations from data has significantly boosted the uptake by the community. This has resulted in diverse deep neural network applications, in which patterns learned from data have been adapted to perform tasks in various domains, including Computer Vision and medical imaging [3,4,5], Signal and Natural Language Processing [6,7,8,9,1]. Traditional image processing techniques have been applied in detection and recognition of text regions with good levels of success. These include include Stroke Width Transform (SWT) [10] and Maximally Stable Extremal Regions (MSER) [11] algorithms. However, these methods consist of multiple components often requiring appropriate tuning, and are known to under perform with high variability of data points. Current OCV systems in the food packaging industry heavily rely on consistency of date-code format, packaging design and viewing angle, when evaluating printing quality of a known text with respect to (w.r.t.) reference samples. However, this consistency can hardly be expected in real scenarios where factory workers are in charge of the verification process. Deep Learning based methods have recently shown to perform very well in complex text detection tasks. [12] identified candidate text regions and then utilised deep CNN to discard false positives. [13] combined aggregated channel features with CNN to spot text in photographs. In [14], a combination of vertical anchors with a joint Convolutional-Recurrent Neural Network (C-RNN) were used to detect horizontal lines of text.

Given the high variability of food packaging coming from different factories, it becomes very challenging to develop a generalised OCV system. This type of problem has previously been addressed in other domains through various adaptive semi-supervised methods. For a more detailed discussion of these methods we refer the reader to [15,16,17]. Some previous work tackles the adaptation of knowledge learnt from a data generating distribution, to a pool set of unlabelled data - which may or may not come from a different distribution - through deep generative modelling techniques [18,



Fig. 1 Per category examples of images in our datasets. (a) Complete Date (day and month visible). (b) Partial Date (no day visible). (c) Partial Date (no month visible). (d) Unreadable. (e) No date (neither day or month visible).

19,20]. Transfer Learning is a related concept, in which such constraints are explored w.r.t. knowledge transfer in large models [21]. Domain adaptation is a special case of TL, and has become a very popular practice in computer vision in recent years, often involving the adaptation of knowledge between classification tasks and/or distributions [22,23,19]. Despite the important algorithmic improvements developed recently, there are still many adversities in training deep learning models which can be easily adapted to other tasks; the lack of annotated data being one of the contributing factors, as well as computational constraints. Moreover, many recent approaches rely on expert knowledge of complex models, such as generative adversarial networks (GANs), or include high algorithmic complexity, which may reduce the uptake of the methods by the industry.

Beyond the adaptation of knowledge between tasks and distributions presented in coming sections, another related open problem in machine learning is the automated acquirement of annotated data. In the context of our applied domain, the amount of unlabelled data far exceeds that which can be annotated by humans. Furthermore, recent advances in Deep Supervised Learning have proven that training over parameterised models on large amounts of annotated data, significantly increases performance [24]. With that in mind - and despite the high demand for annotated data - deep learning practitioners have not yet explored or leveraged many of deep learning tools for automatic annotation systems. This is evidenced by the scarcity of existing research in the field, when this is compared to other fields [2]. Techniques for automated data annotation typically consist of semi-supervised algorithmic variants, wherein learning systems are often trained on a small initial sample of annotated, and leverage unlabelled data in an attempt to generalise other unlabelled sets over time [25]. However, this is a very challenging problem in practice, and few have attempted to address it with high-dimensional real data thus far [2,26,27]. Possible solutions include variants of classical methods such as

Self-Training [28], Co-Training [29] and Active Learning [30]. Active Learning in particular, requires a data acquisition step wherein a collection of particularly informative data points are selected, and proposed to a human annotator. This step can offer insight into what the smallest subset of data points - representative of the whole data distribution - and thus potentially maximise the learning efficiency of the algorithm. In [2], the authors have recently applied these ideas in the context of deep Bayesian models, computing a measure of uncertainty about their predictions. This property is especially useful for safety-critical applications, such as food package OCV. In this framework, we employ a Bayesian interpretation of Self-Training, in which a deep model provides semi-supervised annotation of real food packaging labels; in this way we reduce the burden of data annotation required to perform OCV.

3 Datasets

Four datasets of food package photographs were collected by a leading food company and provided to us for research purposes. The four sets include 1404, 6739, 1154 and 13948 captured images respectively. In order to produce trainable datasets, a portion of the images was first manually annotated w.r.t. the presence of *use-by* dates, and lack thereof. In the case of unreadable images, in which dates were not discernible from the background - potentially due to heavy distortion, non-homogeneous illumination or blur - were then set aside in a separate category. Conversely, images in which either day or month, or both were missing, were considered as incomplete, and subsequently grouped into their own category. Lastly, images of good quality, reporting the date including both the day and month, were considered as good candidates for OCV. The first three sets of images were annotated as mentioned above to form 5 categories: complete dates, missing day, missing month, no date and unreadable (Table 1), whereas photographs belonging to the fourth dataset were anno-

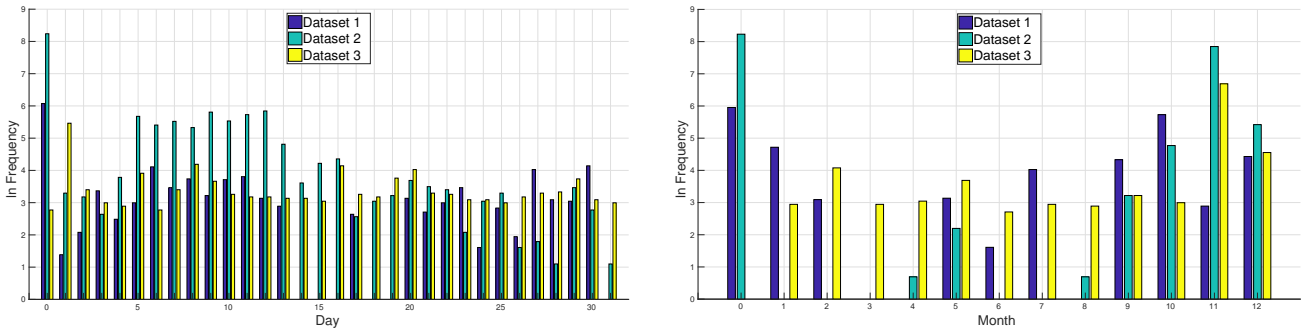


Fig. 2 Left: Frequency (ln scale) of appearance per ‘Day’ in *use-by* dates. **Right:** Respective appearance per ‘Month’.

tated as good or bad candidates for OCV, and utilised to test our proposed Bayesian self-annotating framework. After annotating all the images in the first three datasets, it was possible to plot some statistics (see Figure 2) on the frequency of specific dates within each dataset, and thus devise a methodology for conducting experiments with balanced sets of classes. Moreover, by inspecting the images with partially missing data, it was observed that most of them were photographs of package labels which had been folded at crucial points, included photographic glare, digits fainting over time, or included human made occlusions. With regard to the fourth dataset, 8931 images were annotated as including readable dates, and the remaining 5017 as unreadable.

4 The Proposed Approach

To address the aforementioned challenges, a methodology was devised to develop a robust machine vision solution for automatic date code optical character verification. In our approach, we leverage the feature extraction power inherent to Deep Neural Networks (DNNs) through a combination of transfer learning, k -means clustering and k -Nearest Neighbour classification of Convolutional Neural Network learned representations, and perform adaptation tasks between datasets from different distributions, with the limited and noisy data available. In a complimentary extension of the work, we propose a generalised Deep Bayesian Self-Training framework for tackling semi supervised annotation of real food packaging labels, which can be easily adapted to work on other complex automatic annotation tasks.

4.1 Convolutional Neural Networks

CNN architectures [31, 32] are neural networks that consist of a number convolutional, pooling and fully connected (FC) layers, wherein affine transformations and non-linearities are sequentially applied to the inputs.

The convolutional kernel and FC layer weights are learnt through backpropagation, and the pooling layers are in charge of reducing the dimensionality of the inputs by summarising activations. Typical pre-trained CNN architectures take as input three channelled images and through a series of volume-wise convolutions and feature routing, are capable of selecting near optimal features for the classification of particular objects. This is because deep CNNs stack many non-linearities together and are therefore able to learn very complex hierarchical abstract features with which to represent the data.

4.2 Transfer Learning

It was of particular interest to conduct transfer learning in order to assess the adaptability of pre-trained CNN weights [32] on the current food datasets. Specifically, each image from our datasets was fed through a previously trained InceptionV3 CNN on the ImageNet dataset, up to the last global average pooling (GAP) layer, where a 2048 dimensional vector representation of each instance was extracted. The 2048 dimensional vectors then became the input to a new series of FC layers and a final softmax layer able to predict N classes (see Figure 3). In order to optimise the training performance of the new FC layer network, a series of architectural decisions were made empirically, and the best performances were achieved using a FC network consisting of two 2048 unit hidden layers with Rectified Linear Unit (ReLU) activations and Batch Normalization (BN) [33] layers.

The risk of overfitting rises as the number of parameters increases w.r.t. number of training examples. Due to the limited amount of training data, available for experimentation, it is unfeasible to train state-of-the-art models from scratch. Therefore, we introduced an effective regulariser in the new network as well as adapted previously learned low-level features through transfer learning. One of the most effective regularisation techniques is Dropout [34]. In practice, to preserve more

Table 1 Number of images per category in each dataset.

Annotation (DD/MM)	Dataset		
	1	2	3
Missing/Missing	375	3715	0
Missing/Complete	59	68	16
Complete/Missing	10	39	0
Complete/Complete	645	2847	1138
Unreadable	315	46	0

information in the input layer $\ell^{(0)}$ (of L total layers) in the network and thus aid learning, the probability of keeping ($p(z^{(i)}) \neq 0$) any given neuron $z^{(i)}$ in layer i was as defined per the following schema

$$\ell^{(i)} = \begin{cases} p(z^{(i)}) = 0.8 & \text{if } i = 0 \\ p(z^{(i)}) = 0.5 & \text{otherwise.} \end{cases} \quad (1)$$

In view of the unbalance present among the various classes, it was beneficial to use a weighted negative log-likelihood as a loss function (2). In (2), λ_j is a weight coefficient computed for the j^{th} of all classes J as a function of the proportion of instances N_j compared to the most densely populated class (3). During training, λ encourages the model to focus on under-represented classes

$$\mathcal{L}(\mathbf{y}, \hat{\mathbf{y}}) = - \sum_i \lambda_j \mathbf{y}_i \log \hat{\mathbf{y}}_i - (1 - \mathbf{y}_i) \log(1 - \hat{\mathbf{y}}_i) \quad (2)$$

calculating the per-class weight parameter λ_j with

$$\lambda_j = \frac{1}{N_j} \max \left(\{N_i\}_{i=1:J} \right). \quad (3)$$

In the case of multiclass classification, where $J > 2$, the weighted cross entropy loss function can be defined as

$$\mathcal{L}(\mathbf{y}, \hat{\mathbf{y}}) = - \sum_{i=1}^M \sum_{j=1}^J \lambda_j \mathbf{y}_{ij} \log \hat{\mathbf{y}}_{ij}, \quad (4)$$

where $\log p(\hat{\mathbf{y}} = j | \mathbf{z}_j)$ is calculated as

$$\log softmax(\mathbf{z}_j) = \log \left[\frac{\exp(\mathbf{z}_j)}{\sum_k \exp(\mathbf{z}_k)} \right], \quad (5)$$

\mathbf{z} is a vector of NN output logits, and M denotes the batch size of choice for stochastic optimisation of $\mathcal{L}(\mathbf{y}, \hat{\mathbf{y}})$ via backpropagation. In all cases, we use Adaptive Moment Estimate (Adam) as an optimiser [35].

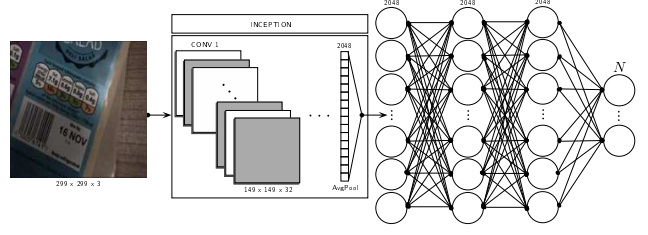


Fig. 3 Depiction of the classification architecture. From left to right, input images were resized to $299 \times 299 \times 3$ to accommodate the CNN’s convolutional layer parameters and arithmetic. There exist 2 hidden layers with 2048 units each and ReLu activations. The number of units N in the softmax layer was adjusted as per the number of classes being classified in different experiments.

4.3 Latent Variable Adaptation of Deep Neural Network Facets

A major challenge spanning the three datasets was the high variability in the captured images characteristics. This variability made the reuse of a DNN trained on one dataset, for classifying the data of another, very difficult leading to poor performances. Fundamentally, this is because each dataset comes from a different distribution, as the images were taken by different people, with different cameras and at differing supplier locations. With limited data available to us, the use of transfer learning among different environments and datasets was ineffective. To overcome these challenges, we demonstrate the possibility of designing a new facet of the same CNN architecture, for learning each considered problem associated with different datasets. The approach focuses on: *i*) detecting bad image capturing conditions; *ii*) detecting missing dates (*i.e.* either day and/or month of *use-by* date); *iii*) showing the ability to recognise day and/or month of an existing *use-by* date.

We propose a new simple methodology for visualising and analysing variability between distributions and attempt to adapt information from one problem to another in DNNs. In Figure 4 an illustration of our adaptation framework is shown. Let the following denote 2 training sets from separate datasets targeting the same task

$$\begin{aligned} \mathcal{D}_1 &= \{(\mathbf{x}_1^{(i)}, \mathbf{y}_1^{(i)}); i = 1, \dots, N_1\} \\ \mathcal{D}_2 &= \{(\mathbf{x}_2^{(i)}, \mathbf{y}_2^{(i)}); i = 1, \dots, N_2\}, \end{aligned} \quad (6)$$

and the respective test sets as

$$\begin{aligned} \mathcal{T}_1 &= \{(\tilde{\mathbf{x}}_1^{(i)}, \tilde{\mathbf{y}}_1^{(i)}); i = 1, \dots, \tilde{N}_1\} \\ \mathcal{T}_2 &= \{(\tilde{\mathbf{x}}_2^{(i)}, \tilde{\mathbf{y}}_2^{(i)}); i = 1, \dots, \tilde{N}_2\}. \end{aligned} \quad (7)$$

Let $\mathcal{F}(\mathcal{D}_1; \mathbf{W}_1)$ and $\mathcal{F}(\mathcal{D}_2; \mathbf{W}_2)$ denote 2 architecturally identical CNNs trained separately on each dataset, from

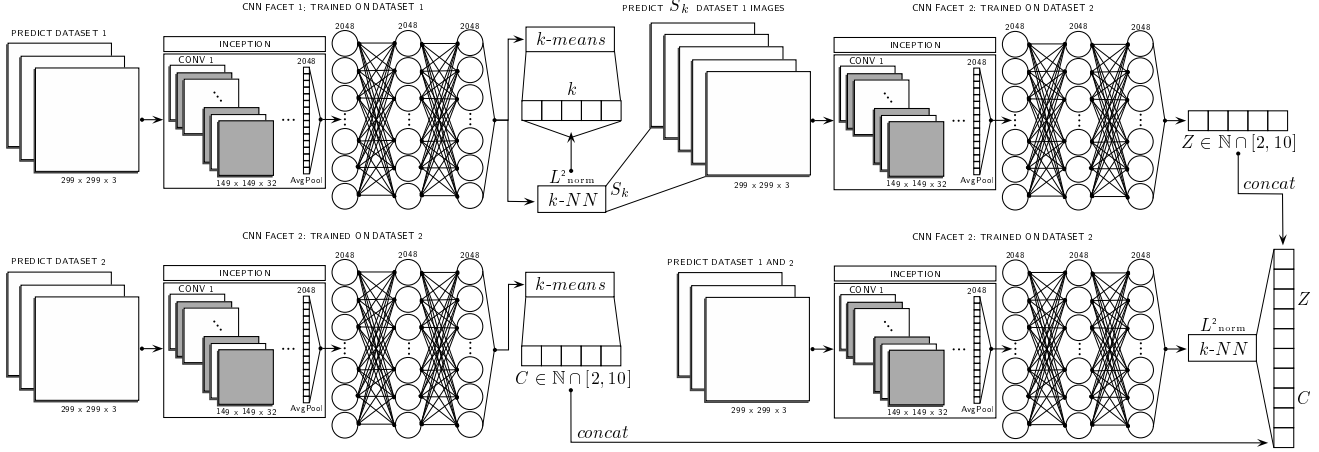


Fig. 4 Illustration of the multiple CNN facet adaptation framework proposed, which is based on clustering of extracted latent variable representations. The architectural details of each CNN are as previously described in Figure 3.

which final FC layer activations $\{\mathbf{x}_1^{(i)}, \tilde{\mathbf{x}}_1^{(i)}\} \in \mathbb{R}^{2048}$ and $\{\mathbf{x}_2^{(i)}, \tilde{\mathbf{x}}_2^{(i)}\} \in \mathbb{R}^{2048}$ were extracted as latent variables obtained through forward-propagation of each image. Our adaptation methodology is then performed as follows

1. Given \mathcal{D}_2 , produce a set of clusters $\mathbf{C} = \{\mathbf{c}_1, \dots, \mathbf{c}_k\}$ by minimising the within-cluster L^2 norms of the following clustering objective function

$$\hat{\mathbf{C}}_{k\text{-means}} = \arg \min_{\mathbf{C}} \sum_{i=1}^k \sum_{\mathbf{x} \in \mathbf{C}_i} \|\mathbf{x} - \boldsymbol{\mu}_i\|^2. \quad (8)$$

2. Repeat step 1 with \mathcal{D}_1 to generate k clusters $\mathbf{U} = \{\mathbf{u}_1, \dots, \mathbf{u}_k\}$, and compute the k closest instances in \mathcal{D}_1 to each centroid in \mathbf{U} . Fetch the corresponding set of images $\mathbf{S} = \{\mathbf{S}_1, \dots, \mathbf{S}_k\}$, whose latent variables are closest to \mathbf{U} ;
3. Forward-propagate \mathbf{S} through $\mathcal{F}(\mathcal{D}_2; \mathbf{W}_2)$ to obtain a new set of adapted clusters $\mathbf{Z} = \{\mathbf{z}_1, \dots, \mathbf{z}_k\}$, where \mathbf{S} is considered an approximation of \mathbf{U} from $\mathcal{F}(\mathcal{D}_1; \mathbf{W}_1)$;
4. Derive an augmented cluster representation that encapsulates knowledge from both facets of the trained CNNs, by concatenating the respective \mathbf{C} and \mathbf{Z} clusters into a set $\mathbf{A} = \{\mathbf{c}_1, \dots, \mathbf{c}_k, \mathbf{z}_1, \dots, \mathbf{z}_k\}$;
5. Compute the euclidean distance between \mathcal{T}_1 and \mathbf{A} and evaluate the classification performance;
6. Iteratively remove the lowest performing cluster in \mathbf{A} and repeat step 5 until the performance stops improving.

In all cases, the k -means++ [36] seeding strategy was used, whereby the first cluster center \mathbf{c}_1 is chosen uniformly at random from \mathcal{X} , and all preceding cluster centers $\mathbf{x} \in \mathcal{X}$ are chosen with probability

$$\mathbf{c}_i = \frac{D(\mathbf{x})^2}{\sum_{\mathbf{x} \in \mathcal{X}} D(\mathbf{x})^2}, \quad (9)$$

where $D(\mathbf{x})$ denotes the distance between \mathbf{x} and the closest \mathbf{c}_i . Moreover, we assign the class label of a given cluster \mathbf{c}_i as simply the mode class j of all data points within it

$$\mathbf{c}_i^j = \max_{j \in J} |\mathbf{c}_i \cap j|. \quad (10)$$

In the experimental study of Section 6, we demonstrate that our method distills and adapts knowledge from both trained CNNs on real data, achieving better performance than direct inference of \mathcal{T}_1 with $\mathcal{F}(\mathcal{D}_2; \mathbf{W}_2)$, without any parameter retraining.

5 Deep Bayesian Self-Training

In this section, we explore the idea of applying Bayesian inference techniques to quantify uncertainty about prediction of pseudo labels, in a real world high-dimensional task, and propose a Deep Bayesian variant of the popular wrapper Self-Training algorithm [28]. As discussed previously, Self-Training is a simple algorithm in which a classifier predicts labels at inference time, and increments the training set with the most confident predictions of the unlabelled data. Our goal is to annotate food package images as being readable or otherwise in an automated manner. Given the safety-critical nature of mislabelling food products, having a measure of uncertainty about our predictions is of great interest to industrial partners, as minimising health risks for customers is paramount.

We begin by defining our backbone NN architecture of choice as a DenseNet [37] pre-trained on ImageNet. DenseNets have revealed several well founded advantages over previous architectures, from mitigating vanishing-gradients, to encouraging feature propa-

gation and reuse with shorter connections between layers [37, 38]. An important side note is that transferring pre-trained features from DenseNet can be very useful in our scenarios, since we start out with a too small training set towards training a state-of-the-art end-to-end architecture. The dense connectivity in DenseNets can be formally defined as

$$\mathbf{A}^{[\ell]} = f \left(\text{BN} \left(\mathbf{W}^{[\ell]} * \left[\mathbf{A}^{[0]}, \mathbf{A}^{[1]}, \dots, \mathbf{A}^{[\ell-1]} \right] \right) \right), \quad (11)$$

where $f(\cdot)$ is the ReLU activation function, $\text{BN}(\cdot)$ is Batch Normalisation [33] and $[\mathbf{A}^{[0]}, \mathbf{A}^{[1]}, \dots, \mathbf{A}^{[\ell-1]}]$ represents feature map-wise concatenation of all layers preceding ℓ . A sequential composite function consisting of BN, ReLU and 3×3 convolution can then be defined as $H^{[\ell]}$. Each function $H^{[\ell]}$ produces ω feature maps, known as the growth rate of the network, and each layer ℓ takes as input $f + \omega \times (\ell - 1)$ total feature maps, where f denotes the number of channels in the visible layer. To reduce spatial dimensionality of feature maps, a Transition layer is introduced between densely connected DenseBlocks. Transition layers in [37] are composed of BN followed by 1×1 convolution and 2×2 average pooling with a feature map compression factor $\theta = 0.5$. In our network, we freeze all layer weights preceding the last DenseBlock in a DenseNet-201 architecture, and replace the 1000 class output layer with a sigmoid neuron for our binary classification task. Further modifications were made to the original network to make it Bayesian, and these are presented in the following subsections.

5.1 Bayesian Convolutional Neural Networks

In order to quantify what our model knows and does not know, we extend existing approaches for estimating uncertainty in deep CNNs [39, 40]. To this end, we consider the following Bayesian formulation of a deep CNN for estimating both aleatoric and epistemic uncertainties.

Let $\mathcal{D} = \{(\mathbf{X}, \mathbf{Y})\}$ denote a dataset given as N pairs of inputs $\mathbf{x}_i \in \mathbb{R}^d$ of dimension d , and class labels $\mathbf{y}_i \in \{1, \dots, K\}$ of K total classes. Assuming a Bayesian Neural Network (BNN) formulation, a prior probability distribution $p(\omega)$ is placed over the set of trainable parameter $\omega = \{\mathbf{W}_1, \dots, \mathbf{W}_\ell\}$, with a Gaussian prior distribution $\omega \sim p(\omega)$ as a sensible choice. We can also define the likelihood conditional output distribution $p(\mathbf{Y}|\mathbf{X}, \omega)$ of our model from mapping inputs to labels, by finding parameters ω that yield the Maximum Likelihood Estimate (MLE). MLE is the pillar of

supervised learning in DNNs and is defined as

$$\hat{\omega}_{\text{ML}} = \arg \max_{\omega} \sum_{i=1}^N \log p(\mathbf{y}_i | \mathbf{x}_i, \omega), \quad (12)$$

giving us a point estimate for the most likely parameters that generated the data. In a Bayesian sense, the MLE is a special case of Maximum A Posteriori (MAP) estimation when a uniform prior is assumed. In practical classification tasks, the MLE estimator is obtained by minimising the negative log-likelihood of a Bernoulli or softmax distribution depending on the number of classes. We define the softmax log-likelihood of our classification model as

$$-\log p(\mathbf{y}_i = k | \mathbf{x}, \omega) = - \left(\mathbf{z}_k - \log \sum_{k'} \exp(\mathbf{z}_{k'}) \right) \quad (13)$$

where \mathbf{z} denotes the vector of output logits by the network and k denotes a class. Having defined a prior and a likelihood for our model, we would like to compute the posterior probability distribution over the weights given the data by Bayes rule

$$p(\omega | \mathbf{X}, \mathbf{Y}) = \frac{p(\mathbf{Y} | \mathbf{X}, \omega) p(\omega)}{p(\mathbf{Y} | \mathbf{X})} \propto p(\mathbf{Y} | \mathbf{X}, \omega) p(\omega), \quad (14)$$

with which we can also formulate the predictive distribution given new inputs \mathbf{x}^* and labels \mathbf{y}^*

$$p(\mathbf{y}^* | \mathbf{x}^*, \mathbf{X}, \mathbf{Y}) = \int p(\mathbf{y}^* | \mathbf{x}^*, \omega) p(\omega | \mathbf{X}, \mathbf{Y}) d\omega, \quad (15)$$

allowing us to make predictions using a full distribution over the parameters ω rather than using a point estimate, capturing uncertainty over the model parameters. The challenge is that, for most of the models we care about, the posterior distribution $p(\omega | \mathbf{X}, \mathbf{Y})$ cannot be evaluated analytically. This is because the marginal probability $p(\mathbf{Y} | \mathbf{X})$ requires us to integrate over all possible model parameters ω with weighted probability $p(\omega)$ to obtain the normalising constant, also known as the model evidence.

Since the true posterior distribution $p(\omega | \mathbf{X}, \mathbf{Y})$ is intractable, various approximations exist [41, 42, 43]. Most of them were important early steps towards performing approximate inference in Bayesian NNs, but are unfortunately difficult to employ in modern applications due to scalability constraints or expert knowledge requirements. More recent work in [40, 44, 45, 46] addressed some of these issues with variational inference, reigniting interest in the field of Bayesian NNs. We employ some of the ideas presented in [40], wherein Dropout is performed at test time to perform a Monte Carlo approximation of the posterior distribution of the parameters given the data.

Formally, we define a variational distribution from a tractable family $q_\theta(\omega)$, parameterised by θ , for approximating the posterior distribution by minimising the Kullback-Leibler (KL) divergence between $q_\theta(\omega)$ and $p(\omega|\mathbf{X}, \mathbf{Y})$. Intuitively, the KL divergence is a non-negative asymmetric measure of similarity between two distributions

$$\text{KL}(q_\theta(\omega) \parallel p(\omega|\mathbf{X}, \mathbf{Y})) = - \int q_\theta(\omega) \log \left\{ \frac{p(\omega|\mathbf{X}, \mathbf{Y})}{q_\theta(\omega)} \right\} d\omega, \quad (16)$$

which we minimise via the variational parameters θ of our approximating distribution $q_\theta(\omega)$

$$\begin{aligned} \hat{\theta} &= \arg \min_{\theta} \mathbb{E}_{q_\theta(\omega)} \left[\log q_\theta(\omega) - \log p(\omega|\mathbf{X}, \mathbf{Y}) \right] \\ &= \arg \min_{\theta} \text{KL}(q_\theta(\omega) \parallel p(\omega|\mathbf{X}, \mathbf{Y})). \end{aligned} \quad (17)$$

However, optimising the KL divergence directly requires knowledge of the intractable posterior. We can circumvent this by instead maximising the variational evidence lower bound (ELBO) on the marginal log-likelihood $\log p(\mathbf{Y}|\mathbf{X})$

$$\mathcal{L}_{\text{ELBO}}(\theta) = \log p(\mathbf{Y}|\mathbf{X}) - \text{KL}(q_\theta(\omega) \parallel p(\omega|\mathbf{X}, \mathbf{Y})), \quad (18)$$

given that the KL divergence is non-negative then

$$\log p(\mathbf{Y}|\mathbf{X}) = \mathcal{L}_{\text{ELBO}}(\theta) + \text{KL}(q_\theta(\omega) \parallel p(\omega|\mathbf{X}, \mathbf{Y})). \quad (19)$$

By maximising the lower bound we implicitly maximise $\log p(\mathbf{Y}|\mathbf{X})$, and minimise the KL divergence as intended. We extend these ideas in light of recent developments in [40] with the *MC Dropout* approximation using $q_\theta(\omega)$ further explained in the following section. First, it is important to note what types of uncertainties we can estimate.

Aleatoric uncertainty relates to sensory noise in the acquisition process of the data, and is therefore inherently irreducible. However, it can be a great tool for modelling noise in the inputs and quantifying our uncertainty about predictions. Contextually, the photographs taken by factory operatives contain various degrees of blur, lighting and viewpoint variability, which can be considered irreducible sensory noise. On the other hand *Epistemic* uncertainty relates to our uncertainty about the model parameters, which is in fact reducible as we observe more data. This is because we can explain the uncertainties about the model parameters in the limit of observing all explanatory variables of the data. This type of uncertainty is mostly useful for identifying out-of-distribution data points.

5.2 Continuous Relaxation of Dropout

Concrete Dropout is based on concrete relaxation of discrete distributions, allowing the replacement of Dropout's discrete Bernoulli distribution with its continuous relaxation [47]. [40] demonstrated that Dropout [48] is a practical tool to perform approximate inference (derive a predictive distribution), which is required to estimate prediction uncertainty. Dropout inference involves the use of Dropout at training time, as well as test time, making use of Dropout masks to generate Monte Carlo samples and approximate the posterior. However, to obtain accurate uncertainty estimates, it is necessary to *ad-hoc* calibrate Dropout probabilities on the available data. A grid-search over Dropout probabilities is a common approach, but costly for large models, highlighting the benefit of optimising them directly with *Gradient Descent*. This requires formulating an objective for minimising the epistemic uncertainty [40] w.r.t. the variational interpretation of Dropout.

Formally, Dropout can be treated as an approximating distribution $q_\theta(\omega)$ to the posterior in a BNN, where ω represents the weight matrices of the l^{th} of L layers in the network $\omega = \{\mathbf{W}_l\}_{l=1}^L$, and θ the variational parameters which the optimisation is performed over. If we let \mathbf{f}^ω be the model with weight matrix realisation ω ; given a random set S comprising M of all N data points, and denoted model's output on the \mathbf{x}_i input as $\mathbf{f}^\omega(\mathbf{x}_i)$, it is possible to formulate the following optimisation objective function

$$\hat{\mathcal{L}}_{\text{MC}}(\theta) = -\frac{1}{M} \sum_{i \in S} \log p(\mathbf{y}_i | \mathbf{f}^\omega(\mathbf{x}_i)) + \frac{1}{N} \text{KL}(q_\theta(\omega) \parallel p(\omega)), \quad (20)$$

where $p(\mathbf{y}_i | \mathbf{f}^\omega(\mathbf{x}_i))$ is model's likelihood, which can be approximated with *e.g.* a Gaussian with mean $\mathbf{f}^\omega(\mathbf{x}_i)$. KL is a regularisation term which constrains the approximate posterior $q_\theta(\omega)$ from deviating too far from prior $p(\omega)$. Following [49] we can approximate the KL term closely with

$$\text{KL}(q_M(\mathbf{W}) \parallel p(\mathbf{W})) \propto \frac{l^2(1-p)}{2} \|\mathbf{M}\|^2 - K\mathbb{H}(p), \quad (21)$$

where $\{\mathbf{M}_l, p_l\}_{l=1}^L$ is a set of mean weight matrices and Dropout probabilities, such that (s.t.) $q_{M_l}(\mathbf{W}_l)$ is equal to $\mathbf{M}_l \cdot \text{diag}[\text{Bernoulli}(1-p_l)^{K_l}]$ for a weight matrix $\mathbf{W}_l \in \mathbb{R}^{K_{l+1} \times K_l}$. $\mathbb{H}(p)$ is the entropy of a Bernoulli random variable with probability p

$$\mathbb{H}(p) := -p \log p - (1-p) \log(1-p). \quad (22)$$

The latter can be interpreted as a regularisation term, and since it only depends on Dropout probability p ,

minimising the KL term is the same as maximising the entropy of a Bernoulli random variable with probability $(1-p)$. However, rather than sampling the random variable from the discrete Bernoulli distribution, by adopting the Concrete distribution [47] with some temperature t , it is possible to sample variables in $[0, 1]$, s.t. the Concrete relaxation distribution $\tilde{\mathbf{z}}$, parametrised by means of $u \sim \text{Unif}(0, 1)$ providing a relationship between $\tilde{\mathbf{z}}$ and u , which is differentiable w.r.t. p .

$$\tilde{\mathbf{z}} = \text{sigmoid}\left(\frac{1}{t} \cdot (\log p - \log(1-p) + \log u - \log(1-u))\right). \quad (23)$$

5.3 Entropy Penalty on Confident Output Distributions

The probabilities assigned to incorrect classes at test time help quantify a model’s ability to generalise. [50] demonstrated that by penalising output distributions with low entropy (i.e. confident predictions), we can obtain a similar effect to label smoothing and improve generalisation. This is especially useful for our setting, whereby we assign pseudo labels based on confident (certain) predictions from our Bayesian Self-Training NN, which are in some cases wrongly assigned labels. We find that by penalising very confident output distributions from our BNN we can improve generalisation, and most importantly, we can better threshold over our predicted labels since the output distributions are smoother rather than overly concentrated at 0 or 1. The entropy of a NNs output conditional distribution can be defined as

$$\mathbb{H}[p(\mathbf{y}|\mathbf{x}, \boldsymbol{\omega})] = - \sum_i p(\mathbf{y}_i|\mathbf{x}, \boldsymbol{\omega}) \log p(\mathbf{y}_i|\mathbf{x}, \boldsymbol{\omega}), \quad (24)$$

with $p(\mathbf{y}|\mathbf{x}, \boldsymbol{\omega})$ as the probability distribution obtained from a softmax function. To penalise very confident predictions we can simply take the negative log-likelihood and subtract the entropy of the output distribution, scaled by a balancing hyperparameter β that controls how much we’d like to penalise non-uniformity

$$\mathcal{L}(\boldsymbol{\omega}) = - \sum \log p(\mathbf{y}|\mathbf{x}, \boldsymbol{\omega}) - \beta \mathbb{H}[p(\mathbf{y}|\mathbf{x}, \boldsymbol{\omega})]. \quad (25)$$

5.4 Inverse Uncertainty Weighting

A widely known limitation of wrapper algorithms, such as Self-Training, is the propagation of errors over time. Its benefit is that it can be adapted to work with most

applications, at the expense of no convergence guarantee. A standard approach to deal with propagating errors is to simply remove less confident data points from the training set, and add them back into the pool of unlabelled data. However, this approach tends to underperform in practice, and the algorithm may become *lazy* by continuously selecting and adding the easiest unlabelled examples to the training set. This can of course hinder the learning of more complex relationships in the data over time, by neglecting the more difficult and potentially highly informative data points.

In attempt to mitigate this behaviour, we propose a sample-wise weighting scheme during training that places a weight on each training sample $(\tilde{\mathbf{x}}_i, \tilde{\mathbf{y}}_i)$, according to the normalised $[0, 1]$ predictive uncertainty σ_i^2 over its predicted label $\tilde{\mathbf{y}}_i$, such that its contribution to the loss function is reduced for more uncertain predictions of the labels

$$\lambda_i = 1 - \log(1 + \sigma_i^2)^{-\phi}, \quad (26)$$

where $\phi(\cdot)$ is a parameterised hyperbolic tangent function

$$\phi(t) = \frac{1 - \exp(-2(\alpha \cdot t - \beta))}{1 + \exp(-2(\alpha \cdot t - \beta))}, \quad (27)$$

whereas α and β are intercept terms and t denotes the current Self-Training iteration. By tuning α and β we can obtain the desired behaviour over t iterations, s.t. when the uncertainty is low we assign high weight to the predicted pseudo label sample $(\tilde{\mathbf{x}}_i, \tilde{\mathbf{y}}_i)$. In other words we are incrementally encouraging the model to assign more weight to uncertain pseudo label samples as training progresses. This is because for small t at the beginning of training, $\phi(t) \approx 1$ and converges to -1 as t approaches infinity. Intuitively, this has the effect of inverting eq. (26) over time, thus encouraging the model to take risks by selecting more uncertain and potentially informative samples to add to the training set.

6 Experimental Study

Five sets of experiments were conducted and the obtained results are reported in Tables 2, 3, 4 and 5.

The goal of the *first* experiment was to establish a baseline for images that would be classified as acceptable according to human standards. As explained in section 1, some of the implications of such an automated system include the elimination of tedious manual labour, reduced human error in package management and routing, increased speed and productivity, while providing statistically significant correctness rates. For the most

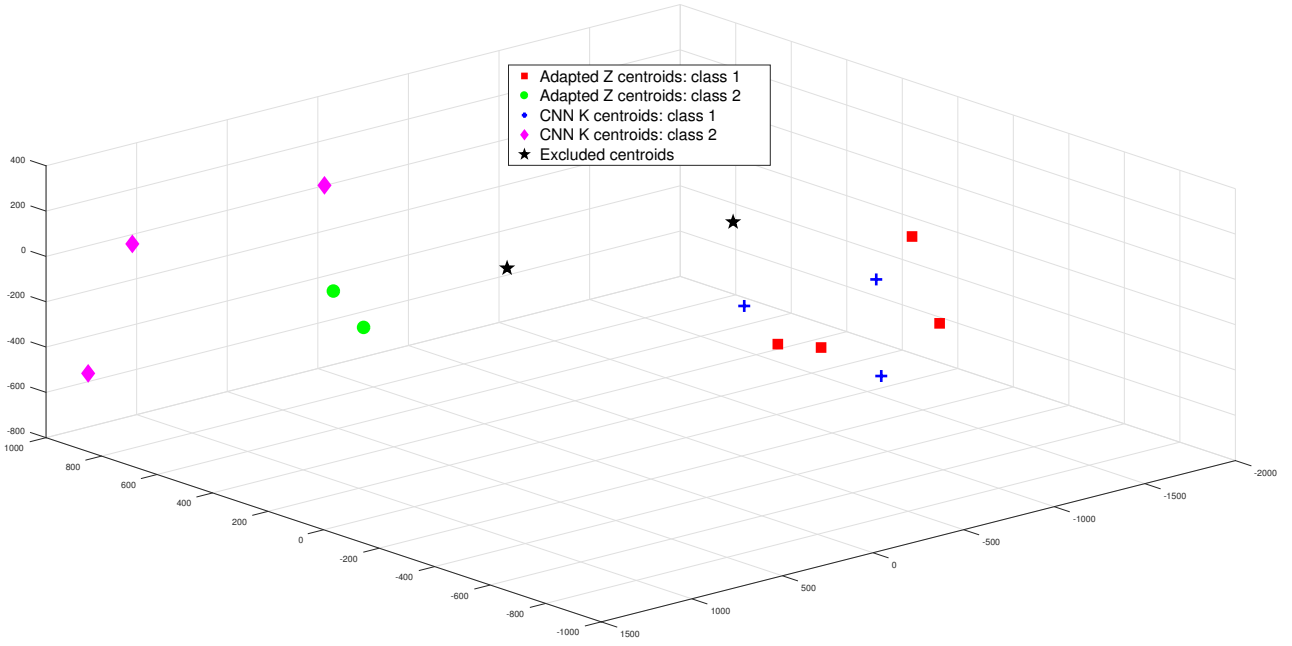


Fig. 5 t-SNE visualisation of the derived centroids \mathbf{A} with best $k = 7$, achieving the results reported in Table 4. The ‘Excluded centroids’ (2 black stars) were removed as per the policy outlined in step 6 of our proposed adaptation procedure.

part, images which were annotated as unreadable contained some form of heavy distortion such as photographic glare or blur, which rendered dates indiscernible from the background. Consequently, these must be filtered from the set of acceptable images and not be considered for further OCV processing.

The *second* experiment aimed at distinguishing between acceptable and not-acceptable, missing dates. For this purpose, it was imperative to ensure that partial dates were not accepted by this process. This meant that the absence of either day or month digits in a *use-by* date, had to be identified and filtered from the set of acceptable images. Moreover, in many cases the partially missing date digits/letters could be present elsewhere in the image, and misclassification of these occurrences would lead to partial dates being processed as acceptable and affect the accuracy of the system.

In a brief *third* experiment, a global approach to OCV was tested by targeting the classification of specific digits and letters. Successful text recognition systems typically begin with the detection of text presence within a given image, followed by a segmentation or localisation of the desired region-of-interest (ROI) in order to perform classification of segmented digits thereafter. In this short study, we assess how well the NN can perform without specifying any additional labels or local information.

In the *fourth* experiment, we examined the ability of the proposed latent variable adaptation approach described in section 4.3, to improve the classification per-

formance of a DNN trained on one of the datasets and tested on another.

Lastly, the *fifth* experiment consists of evaluating our proposed Deep Bayesian Self-Training approach for automatic data-annotation on the food package datasets. We demonstrate the advantages of quantifying uncertainty in deep models and provide a comparison with standard Self-Training methods on complex image data.

It is important to note that in all cases, our developed systems have been tuned to perform well in our application domain, but many of the ideas presented in this paper can be generalised and extended to perform adaptation or self-annotation of other datasets from different tasks.

6.1 Experiment 1: Complete vs Unreadable Dates

As a result of the annotation policy outlined in section 3, the appearance of unreadable images was especially prominent in the 1st of the three datasets. Conversely, the average image quality of the 2nd and 3rd datasets was higher, therefore they were not considered in this experiment. Moreover, the 1st dataset contained images from seven different locations, and as such, there were at least seven different types of food packaging present. To devise a balanced experiment, images from all locations were combined and categorised into 2 classes: ‘Complete Dates’ and ‘Unreadable’. The images were

Table 2 Experiment results of OCV binary classification.

CNN Optical Character Verification				
Exper.	Dataset	OK	NOT-OK	Accuracy (%)
1	1	645	645	90.1%
2	1	645	444	89.3%
	2	2847	2847	96.8%
	3	577	577	85.8%
2.1	1	714	375	94.8%
	2	2954	2954	96.2%
	3	199	199	88.1%

Table 3 Experiment results for date character recognition.

CNN Date Character Recognition			
Exper.	Dataset	Images per Class	Accuracy (%)
3	2	381, 381, 381	92.7%
	3	55, 67, 63, 61	90%

then fed through the CNN described in the former Section and their respective 2048 dimensional vector representations were extracted. Utilising these vector representations, the last fully-connected layers of the network (see section: 4) were trained by Backpropagation using our class labels. As reported in Table 2, **90.1%** classification accuracy was achieved over all seven locations.

6.2 Experiment 2: Complete vs Partial Dates

In this experiment, the previously discussed issue of misleading partial dates was studied. The 2nd dataset was the largest, containing approximately 50% of examples with partial or missing dates. Images missing the day/month or both were assigned to one class and ‘Complete Dates’ to the other. As reported in Table 2, an accuracy of **96.8%** was achieved. Similarly, although using significantly fewer training examples, a performance of **94.8%** was achieved when applying the same procedure to the 1st dataset. A similar experiment was conducted on the 3rd dataset, which includes images of higher quality. However, a very small number of missing value examples were included in this dataset. To address this issue, we performed data augmentation in order to produce a larger set of ‘Partial Dates’ with which we could then formulate our classification task. The accuracy achieved on this synthetic set was **85.8%**.

Lastly, a small variation of this experiment (2.1 in Table 2) was conducted in order to assess how well the network can identify the presence of any type of date, be it complete or partial, versus the absence of a date altogether. This experiment offered insight into how well the network can produce inferred localisation of dates,

Table 4 Experiment results of our adaptation procedure.

Latent Variable Adaptive Clustering		
Test Dataset	Classification Accuracy (%)	
	CNN $\mathcal{F}(\mathcal{D}_2; \mathbf{W}_2)$	Our Method (A)
\mathcal{T}_1	63.8%	76.4%
\mathcal{T}_2	95.9%	97.1%

as it must learn to filter out the abundant non-date related text/numbers in the images. Table 2 shows that good accuracies were achieved across all three datasets, with the best case of **96.2%** date presence detection on the 2nd dataset.

6.3 Experiment 3: Date Character Recognition

Given that almost all images in the 3rd dataset contained ‘Complete Dates’, it was possible to conduct the global approach to OCV previously explained in section 6, and perform a brief digit classification experiment (see Table 3 for results). Despite the small number of training examples (1138) and limited possible class combinations, four digit classes were identified, namely: 5, 8, 16 and 20. With these labelled examples, an accuracy of **90%** was achieved. Similarly for the 2nd dataset - due to limited data - a brief global OCV classification experiment between the the months of October and November in *use-by* dates was conducted. An accuracy of **92.7%** was achieved despite the small number of training examples. In reflection of these results, it is important to remember the great variety of text and numbers included in each image. Without providing any local knowledge and given limited training examples, the networks were still able to automatically infer the importance of specific digits and their respective locations in a global manner, whilst ignoring the same or other digits located in close proximity.

6.4 Experiment 4: Latent Variable Adaptive Clustering

The CNN architectures proved to be quite accurate in identifying the missing/complete dates classification problem. Subsequently, we explored whether the respective trained networks were suitable for carrying out the proposed network adaptation approach described in Section 4.3 (see Table 4 for results).

To this end, consider $\mathcal{F}(\mathcal{D}_2; \mathbf{W}_2)$ as a trained CNN with a test performance of 95.9% on a binary classification problem of *use-by* date verification on a real dataset. Let \mathcal{T}_1 be the test set of a dataset from a different

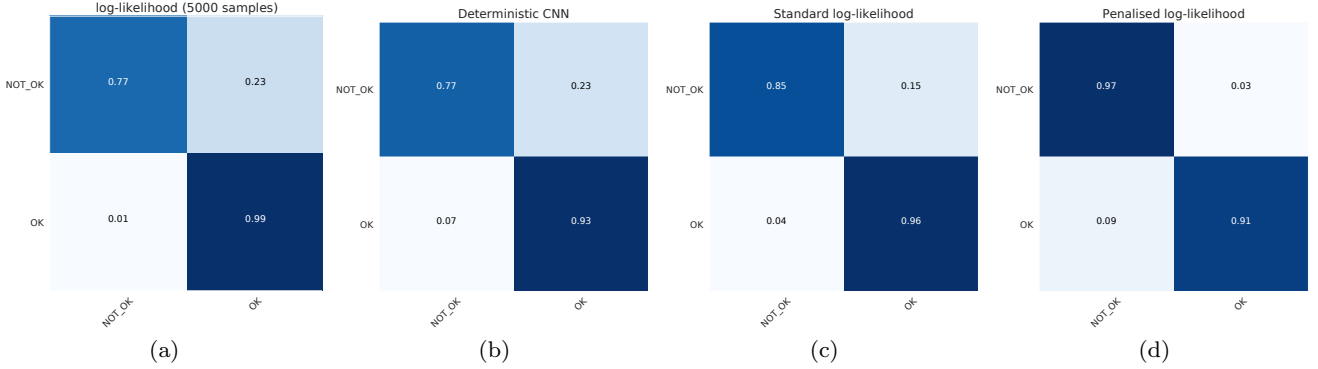


Fig. 6 Normalised confusion matrices of the results obtained from our self-annotation procedure. \mathbf{x} and \mathbf{y} axes denote the *predicted* and *actual* classes, respectively. **(a)** Refers to the 5000 predicted labels obtained with the lowest prediction uncertainty. **(b)** Deterministic CNN predicted labels, wherein the thresholds were set based on networks sigmoidal output. **(c)** Predicted labels from our Bayesian Self-Training approach, trained with a standard binary log-likelihood loss. **(d)** Similar to (c) but using a Bayesian CNN trained with a penalised binary log-likelihood loss rather than the standard.

distribution targeting the same classification task. We forward-propagate \mathcal{T}_1 through $\mathcal{F}(\mathcal{D}_2; \mathbf{W}_2)$ and achieve a lower accuracy of 63.8% as expected. We employed our adaptation procedure to classify \mathcal{T}_1 without any parameter retraining, decreasing the relative error by 34.81% with an improved accuracy of **76.4%**. Interestingly, the original performance achieved by $\mathcal{F}(\mathcal{D}_2; \mathbf{W}_2)$ on \mathcal{T}_2 also increased from 95.9% to **97.1%** when classifying \mathcal{T}_2 with \mathbf{A} instead of the CNN it was originally trained on. Figure 5 depicts a 3D visualisation of all 2048-dimensional cluster centroids, for $k = 7$ for both datasets (14 in total). Squares (Red) and (Blue) crosses denote the centroids corresponding to the complete date class in the first and second datasets respectively. (Green) circles and (Pink) diamonds are the centroids in the missing date category and the (Black) stars indicate the centroids not used in the final classification as per the centroid exclusion policy explained previously in section 4.3.

6.5 Experiment 5: Deep Bayesian Self-Training

In order to validate our approach to automatic annotation, we conducted a series of experiments on a pool of held-out annotated data comprised of 11948 food package images. The results can be seen in Table 5 and Figure 6. We begin by introducing Concrete Dropout layers after every convolutional layer in the last DenseBlock of a DenseNet-201, pre-trained on ImageNet. We then fine-tuned the last DenseBlock on a small portion of 500 images, with binary annotated labels representing whether the *use-by* date was readable (OK) or not (NOT-OK).

Post training, we performed the approximate variational inference method outlined in section 4 by using

Dropout at test time, and run $T = 50$ Monte Carlo samples in order to approximate the predictive distribution. After drawing and obtaining these samples, predictive uncertainty was quantified following [51] as

$$\frac{1}{T} \sum_{t=1}^T \text{diag}(p(\hat{\omega}_t)) - p(\hat{\omega}_t)^{\otimes 2} + \frac{1}{T} \sum_{t=1}^T \left(p(\hat{\omega}_t) - \frac{1}{T} \sum_{t=1}^T p(\hat{\omega}_t) \right)^{\otimes 2}, \quad (28)$$

where $p(\hat{\omega}_t)$ is the softmax output of the network at iteration t , and $\{\hat{\omega}\}_{t=1}^T$ are a set of realised vectors randomly drawn from the variational distribution $q_{\hat{\theta}}(\omega)$ imposed by the different Dropout masks at test time. The first term refers to the irreducible *aleatoric* uncertainty and the second term refers to the *epistemic* uncertainty over model’s parameters. The sum of the two gives us a predictive uncertainty per datapoint, which can be leveraged to discard predicted labels that the BCNN is unsure about.

As observable in Figure 6a, we first applied these ideas to the full set of unlabelled 11948 images and simply selected the 500 most certain predicted labels to be added to the initial training set of 500 images. This process was repeated 10 times in order to collect a total of 5000 images with predicted labels, which we then compared with our annotated labels as shown in Table 5. In the remaining set of experiments, instead of selecting a pre-determined number of images, we filtered out uncertain predictions based on a threshold. Figures 6c and 6d depict the confusion matrices for the automatically annotated images w.r.t. true labels, and highlight the benefits of applying a confidence penalty on the log-likelihood loss, as opposed to using a standard log-likelihood which often outputs overconfident distribu-

Table 5 Bayesian Self-Training for automatic annotation.

Bayesian CNN (Penalised log-likelihood)				
Cohen’s Kappa: 0.8891				
Class	Precision	Recall	F1	#Images
NOT-OK	0.9532	0.9694	0.9612	294
OK	0.9427	0.9136	0.9279	162
Avg./Total	0.9494	0.9496	0.9494	456

Bayesian CNN (Standard log-likelihood)				
Cohen’s Kappa: 0.8383				
Class	Precision	Recall	F1	#Images
NOT-OK	0.9679	0.8538	0.9073	212
OK	0.889	0.9764	0.9306	254
Avg./Total	0.9248	0.9206	0.9200	466

Deterministic CNN (Standard log-likelihood)				
Cohen’s Kappa: 0.6964				
Class	Precision	Recall	F1	#Images
NOT-OK	0.9158	0.7682	0.8355	453
OK	0.7989	0.9287	0.8589	449
Avg./Total	0.8576	0.8481	0.8472	902

tions. The predictive uncertainties were normalised to be in the range $[0, 1]$, and the thresholds were set to be close to 0, s.t. only the most stable predictions over the 50 Monte Carlo samples were selected. In order to compare our approach to standard Self-Training, we took the same network and datasets splits, and trained it without the Bayesian components. The threshold was set based on the confidence of the CNN output to only consider predictions with over 0.999 predicted probability. As can be seen in Table 5, the deterministic CNN tends to be overconfident in its wrong predictions. This causes an increase of the propagated error as more images with predicted labels are added to the training set. To ensure a fair comparison between the Self-Training methods, the *stop* conditions were set to be identical s.t. the procedure was interrupted after 3 consecutive iterations without selecting more images to be added to the training set.

7 Conclusions and Future Work

This paper proposed an adaptive deep learning framework which can greatly assist Optical Character Verification. The system aims to automate the identification of *use-by* dates on food packaging labels. Given the scarcity of data available, CNN extracted representations were first clustered using a *k*-means algorithm, followed by a *k*-nearest neighbour adaptation approach

to combine centroids computed for multiple CNNs addressing the same task. By doing this, better separation and adaptation was achieved when classifying representations learned by another CNN on a similar problem, whilst using a different dataset.

We then extended our developments towards OCV of real food packaging image data. A Deep Bayesian Self-Training algorithm was formulated, built upon recent developments in practical variational inference of deep Bayesian Convolutional Neural Network models. We estimate both *aleatoric* and *epistemic* uncertainties about our predicted pseudo-labels, and leverage these uncertainties to mitigate known negative effects of Self-Training, such as propagation of errors over time. We apply an Entropy penalty to the standard log-likelihood loss to punish confident output distributions, and introduce a new *inverse uncertainty weighting* scheme that encourages the model to take risks over time, as opposed to the algorithm repeatedly selecting the easier examples to add to the training set.

The OCV with Deep Learning technologies developed in this paper can enable far greater control over the accuracy and legibility of critical *use-by* dates and also key trace-ability information in food and drink manufacturing operations, resulting in significantly increased food safety and compliance with related legislation. The technology developed may also provide far wider options for advancement of food package control including the confirmation of allergen labelling ‘present and correct’ on pack labels; confirmation that the right packaging has been used for each food pack and that the sales scanning bar code on each pack is readable and correct. Additionally it is necessary to perform quality Control ‘Vision Inspection’ checking that the product in the pack is visually correct.

Our future work will extend the experimental study on larger datasets with the goal to create a fully automated optical verification system for food packaging. A large database, consisting of about half a million food packaging images has been obtained, and the intend to apply the presented deep neural network based methodologies for adaptation and self-annotation of this data.

Acknowledgements The authors would like to thank Mr. George Marandianos, Mrs. Mamatha Thota and Mr. Samuel Bond-Taylor for manually annotating datasets used in this study.

Funding: The research presented in this paper was funded by Engineering and Physical Sciences Research Council (Reference number EP/R005524/1) and Innovate UK (Reference number 102908), in collaboration with the Olympus Automation Limited Company, for the project Automated Robotic Food Manufacturing System.

Conflict of Interest: The authors declare that they have no conflict of interest.

References

1. Fabio De Sousa Ribeiro, Francesco Calivá, Mark Swainson, Kjartan Gudmundsson, Georgios Leontidis, and Stefanos Kollias. An adaptable deep learning system for optical character verification in retail food packaging. In *Evolving and Adaptive Intelligent Systems, IEEE International Conference on*, 2018.
2. Yarin Gal, Riashat Islam, and Zoubin Ghahramani. Deep bayesian active learning with image data. *arXiv preprint arXiv:1703.02910*, 2017.
3. Piotr Chudzik, Somshubra Majumdar, Francesco Calivá, Bashir Al-Diri, and Andrew Hunter. Microaneurysm detection using fully convolutional neural networks. *Computer methods and programs in biomedicine*, 158:185–192, 2018.
4. Fabio De Sousa Ribeiro, Liyun Gong, Francesco Calivá, Mark Swainson, Kjartan Gudmundsson, Miao Yu, Georgios Leontidis, Xujiong Ye, and Stefanos Kollias. An end-to-end deep neural architecture for optical character verification and recognition in retail food packaging. In *2018 25th IEEE International Conference on Image Processing (ICIP)*, pages 2376–2380. IEEE, 2018.
5. Dimitrios Kollias, Miao Yu, Athanasios Tagaris, Georgios Leontidis, Andreas Stafylopatis, and Stefanos Kollias. Adaptation and contextualization of deep neural network models. In *2017 IEEE Symposium Series on Computational Intelligence (SSCI)*, pages 1–8, 2017.
6. Dimitrios Kollias, Athanasios Tagaris, Andreas Stafylopatis, Stefanos Kollias, and Georgios Tagaris. Deep neural architectures for prediction in healthcare. *Complex & Intelligent Systems*, pages 1–13, 2018.
7. Chen Sun, Abhinav Shrivastava, Saurabh Singh, and Abhinav Gupta. Revisiting unreasonable effectiveness of data in deep learning era. In *2017 IEEE International Conference on Computer Vision (ICCV)*, pages 843–852. IEEE, 2017.
8. Francesco Caliva, Fabio De Sousa Ribeiro, Antonios Mylonakis, Christophe Demaziere, Paolo Vinai, Georgios Leontidis, and Stefanos Kollias. A deep learning approach to anomaly detection in nuclear reactors. In *2018 International Joint Conference on Neural Networks (IJCNN)*, pages 1–8, 2018.
9. Fabio De Sousa Ribeiro, Francesco Caliva, Dionysios Chionis, Abdelhamid Dokhane, Antonios Mylonakis, Christophe Demaziere, Georgios Leontidis, and Stefanos Kollias. Towards a deep unified framework for nuclear reactor perturbation analysis. *2018 IEEE Symposium Series on Computational Intelligence (SSCI)*, pages 1–8, 2018.
10. Boris Epshtein, Eyal Ofek, and Yonatan Wexler. Detecting text in natural scenes with stroke width transform. In *Computer Vision and Pattern Recognition (CVPR), 2010 IEEE Conference on*, pages 2963–2970. IEEE, 2010.
11. Huizhong Chen, Sam S Tsai, Georg Schroth, David M Chen, Radek Grzeszczuk, and Bernd Girod. Robust text detection in natural images with edge-enhanced maximally stable extremal regions. In *Image Processing (ICIP), 2011 18th IEEE International Conference on*, pages 2609–2612. IEEE, 2011.
12. Weilin Huang, Yu Qiao, and Xiaoou Tang. Robust scene text detection with convolution neural network induced msr trees. In *European Conference on Computer Vision*, pages 497–511. Springer, 2014.
13. Max Jaderberg, Andrea Vedaldi, and Andrew Zisserman. Deep features for text spotting. In *European conference on computer vision*, pages 512–528. Springer, 2014.
14. Zhi Tian, Weilin Huang, Tong He, Pan He, and Yu Qiao. Detecting text in natural image with connectionist text proposal network. In *European Conference on Computer Vision*, pages 56–72. Springer, 2016.
15. Sinno Jialin Pan, Qiang Yang, et al. A survey on transfer learning. *IEEE Transactions on knowledge and data engineering*, 22(10):1345–1359, 2010.
16. Isaac Triguero, Salvador García, and Francisco Herrera. Self-labeled techniques for semi-supervised learning: taxonomy, software and empirical study. *Knowledge and Information Systems*, 42(2):245–284, 2015.
17. Vishal M Patel, Raghuraman Gopalan, Ruonan Li, and Rama Chellappa. Visual domain adaptation: A survey of recent advances. *IEEE signal processing magazine*, 32(3):53–69, 2015.
18. Diederik P Kingma, Shakir Mohamed, Danilo Jimenez Rezende, and Max Welling. Semi-supervised learning with deep generative models. In *Advances in Neural Information Processing Systems*, pages 3581–3589, 2014.
19. Eric Tzeng, Judy Hoffman, Kate Saenko, and Trevor Darrell. Adversarial discriminative domain adaptation. In *Computer Vision and Pattern Recognition (CVPR)*, volume 1, page 4, 2017.
20. Konstantinos Bousmalis, Nathan Silberman, David Dohan, Dumitru Erhan, and Dilip Krishnan. Unsupervised pixel-level domain adaptation with generative adversarial networks. In *The IEEE Conference on Computer Vision and Pattern Recognition (CVPR)*, volume 1, page 7, 2017.
21. Yoshua Bengio. Deep learning of representations for unsupervised and transfer learning. In *Proceedings of ICML Workshop on Unsupervised and Transfer Learning*, pages 17–36, 2012.
22. Jason Yosinski, Jeff Clune, Yoshua Bengio, and Hod Lipson. How transferable are features in deep neural networks? In *Advances in neural information processing systems*, pages 3320–3328, 2014.
23. Amir R Zamir, Alexander Sax, William Shen, Leonidas Guibas, Jitendra Malik, and Silvio Savarese. Taskonomy: Disentangling task transfer learning. In *Proceedings of the IEEE Conference on Computer Vision and Pattern Recognition*, pages 3712–3722, 2018.
24. Alex Krizhevsky, Ilya Sutskever, and Geoffrey E Hinton. Imagenet classification with deep convolutional neural networks. In *Advances in neural information processing systems*, pages 1097–1105, 2012.
25. Xiaojin Zhu. Semi-supervised learning literature survey. *Computer Science, University of Wisconsin-Madison*, 2(3):4, 2006.
26. Yanyao Shen, Hyokun Yun, Zachary C Lipton, Yakov Kronrod, and Animashree Anandkumar. Deep active learning for named entity recognition. *arXiv preprint arXiv:1707.05928*, 2017.
27. Ozan Sener and Silvio Savarese. Active learning for convolutional neural networks: A core-set approach. *International Conference on Learning Representations*, 2018.
28. David Yarowsky. Unsupervised word sense disambiguation rivaling supervised methods. In *Proceedings of the 33rd annual meeting on Association for Computational Linguistics*, pages 189–196. Association for Computational Linguistics, 1995.
29. Avrim Blum and Tom Mitchell. Combining labeled and unlabeled data with co-training. In *Proceedings of the eleventh annual conference on Computational learning theory*, pages 92–100. ACM, 1998.
30. Burr Settles. Active learning. *Synthesis Lectures on Artificial Intelligence and Machine Learning*, 6(1):1–114, 2012.

31. Yann LeCun, Léon Bottou, Yoshua Bengio, and Patrick Haffner. Gradient-based learning applied to document recognition. *Proceedings of the IEEE*, 86(11):2278–2324, 1998.
32. Christian Szegedy, Vincent Vanhoucke, Sergey Ioffe, Jon Shlens, and Zbigniew Wojna. Rethinking the inception architecture for computer vision. In *Proceedings of the IEEE Conference on Computer Vision and Pattern Recognition*, pages 2818–2826, 2016.
33. Sergey Ioffe and Christian Szegedy. Batch normalization: Accelerating deep network training by reducing internal covariate shift. *arXiv preprint arXiv:1502.03167*, 2015.
34. Nitish Srivastava, Geoffrey Hinton, Alex Krizhevsky, Ilya Sutskever, and Ruslan Salakhutdinov. Dropout: A simple way to prevent neural networks from overfitting. *The Journal of Machine Learning Research*, 15(1):1929–1958, 2014.
35. Diederik P Kingma and Jimmy Ba. Adam: A method for stochastic optimization. *arXiv preprint arXiv:1412.6980*, 2014.
36. David Arthur and Sergei Vassilvitskii. k-means++: The advantages of careful seeding. In *Proceedings of the eighteenth annual ACM-SIAM symposium on Discrete algorithms*, pages 1027–1035. Society for Industrial and Applied Mathematics, 2007.
37. Gao Huang, Zhuang Liu, Laurens Van Der Maaten, and Kilian Q Weinberger. Densely connected convolutional networks. In *CVPR*, volume 1, page 3, 2017.
38. Simon Jégou, Michal Drozdal, David Vazquez, Adriana Romero, and Yoshua Bengio. The one hundred layers tiramisu: Fully convolutional densenets for semantic segmentation. In *Computer Vision and Pattern Recognition Workshops (CVPRW), 2017 IEEE Conference on*, pages 1175–1183. IEEE, 2017.
39. Alex Kendall and Yarin Gal. What uncertainties do we need in bayesian deep learning for computer vision? In *Advances in neural information processing systems*, pages 5574–5584, 2017.
40. Yarin Gal and Zoubin Ghahramani. Dropout as a bayesian approximation: Representing model uncertainty in deep learning. In *international conference on machine learning*, pages 1050–1059, 2016.
41. David JC MacKay. A practical bayesian framework for backpropagation networks. *Neural computation*, 4(3):448–472, 1992.
42. Radford M Neal. *Bayesian learning for neural networks*, volume 118. Springer Science & Business Media, 2012.
43. Geoffrey E Hinton and Drew Van Camp. Keeping the neural networks simple by minimizing the description length of the weights. In *Proceedings of the sixth annual conference on Computational learning theory*, pages 5–13. ACM, 1993.
44. Alex Graves. Practical variational inference for neural networks. In *Advances in neural information processing systems*, pages 2348–2356, 2011.
45. Max Welling and Yee W Teh. Bayesian learning via stochastic gradient langevin dynamics. In *Proceedings of the 28th International Conference on Machine Learning (ICML-11)*, pages 681–688, 2011.
46. Diederik P Kingma and Max Welling. Auto-encoding variational bayes. *arXiv preprint arXiv:1312.6114*, 2013.
47. Chris J Maddison, Andriy Mnih, and Yee Whye Teh. The concrete distribution: A continuous relaxation of discrete random variables. *arXiv preprint arXiv:1611.00712*, 2016.
48. Geoffrey E Hinton, Nitish Srivastava, Alex Krizhevsky, Ilya Sutskever, and Ruslan R Salakhutdinov. Improving neural networks by preventing co-adaptation of feature detectors. *arXiv preprint arXiv:1207.0580*, 2012.
49. Yarin Gal. Uncertainty in deep learning. *University of Cambridge*, 2016.
50. Gabriel Pereyra, George Tucker, Jan Chorowski, Łukasz Kaiser, and Geoffrey Hinton. Regularizing neural networks by penalizing confident output distributions. *arXiv preprint arXiv:1701.06548*, 2017.
51. Yongchan Kwon, Joong-Ho Won, Beom Joon Kim, and Myunghee Cho Paik. Uncertainty quantification using bayesian neural networks in classification: Application to ischemic stroke lesion segmentation. *Medical Imaging with Deep Learning*, 2018.